

Giant anomalous Nernst effect in the $\text{Co}_2\text{MnAl}_{1-x}\text{Si}_x$ Heusler alloy induced by Fermi level tuning and atomic ordering

Y. Sakuraba^{1,2,*}, K. Hyodo,³ A. Sakuma,³ and S. Mitani¹

¹Research Center for Magnetic and Spintronic Materials, National Institute for Materials Science, Sengen 1-2-1, Tsukuba, Ibaraki 305-0047, Japan

²PRESTO, Japan Science and Technology Agency, Saitama 332-0012, Japan

³Department of Applied Physics, Tohoku University, Aoba-ku, Sendai 980-8579, Japan



(Received 30 October 2019; accepted 9 March 2020; published 6 April 2020)

Co_2MnAl has been predicted to have Weyl points near the Fermi level in $L2_1$ -ordered structure, which is expected to give rise to exotic transverse transport properties such as large anomalous Hall (AHE) and Nernst effects (ANE) due to large Berry curvature. In this study, the effects of Fermi level position and atomic ordering on AHE and ANE in $\text{Co}_2\text{MnAl}_{1-x}\text{Si}_x$ were studied systematically. The Co_2MnAl film keeps $B2$ -disordered structure regardless of annealing temperature, which results in much smaller anomalous Hall conductivity σ_{xy} and transverse Peltier coefficient α_{xy} than those calculated for $L2_1$ -ordered Co_2MnAl . Our newly performed calculation of σ_{xy} with taking $B2$ disordering into account well reproduces the experimental result; thus it was concluded that Berry curvature originating from the Weyl points is largely reduced by $B2$ disordering. It was also revealed Al substitution with Si shifts the position of the Fermi level and greatly improves the $L2_1$ atomic ordering, leading to strong enhancement of α_{xy} , which also agreed with our theoretical calculation. The highest thermopower of ANE of $5.7 \mu\text{V}/\text{K}$, which is comparable to the recent reports for Co_2MnGa , was observed for $\text{Co}_2\text{MnAl}_{0.63}\text{Si}_{0.37}$ because of dominant contribution of α_{xy} . This study clearly shows the importance of both Fermi level tuning and high atomic ordering for obtaining the effect of topological features in Co-based Heusler alloys on transverse transport properties.

DOI: [10.1103/PhysRevB.101.134407](https://doi.org/10.1103/PhysRevB.101.134407)

I. INTRODUCTION

The anomalous Nernst effect (ANE), which is a thermoelectric phenomenon unique to magnetic materials, has attracted attention because of several unique advantages for thermoelectric applications [1–3]. Here, the electric field of ANE (\vec{E}_{ANE}) can be expressed by the following equation:

$$\vec{E}_{\text{ANE}} = S_{\text{ANE}} \nabla T \times \left(\frac{\vec{M}}{|\vec{M}|} \right), \quad (1)$$

where S_{ANE} and \vec{M} represent the anomalous Nernst thermopower and magnetization, respectively. As Eq. (1) indicates, ANE generates an electric field in the direction of the outer product of the magnetization \vec{M} and temperature gradient ∇T . This three dimensionality of ANE enables us to increase the serial voltage by using thermopiles consisting of simple laterally connected magnetic wires, because \vec{E}_{ANE} appears along the surface of a heat source. This is a significant advantage for enlarging the size of the thermoelectric power generation module and utilizing large-area of nonflat heat sources. In addition to such attractive features for practical applications, recent findings of large ANE originating from the materials having topological features such as Mn_3Sn [4] stimulated studies on ANE for gaining a fundamental understanding of the phenomenon and enhancing its thermopower [3,5–20]. It has

been recently reported that the ferromagnetic Heusler alloy Co_2MnGa showed the largest S_{ANE} of about $6 \mu\text{V}/\text{K}$ [7,8], which is one order of magnitude larger than that the conventional ferromagnets in Fe, Co, and Ni [21]. Such large thermopower was explained as an exotic property of a magnetic Weyl semimetal in Co_2MnGa . Namely, a large transverse thermoelectric effect intrinsically appears in Co_2MnGa due to its large Berry curvature near the Fermi level (E_F) because of the formation of Weyl points on the nodal lines of electronic bands by the spin-orbit interaction [6,8,9]. Such a topological feature of magnetic material has attracted worldwide interest for not only fundamental physics but also its great potential of practical applications. One curious issue yet to be clarified in Heusler alloy-based Weyl semimetals is how the atomic ordering and the position of E_F against the Weyl points affects the sign and magnitude of ANE. Since previous studies for ANE in Heusler alloy-based Weyl semimetals have focused on the bulk single crystal or epitaxial thin film having high $L2_1$ atomic ordering and the stoichiometric composition [7,8], it is still unclear how much ANE is sensitive to the atomic ordering and chemical composition both theoretically and experimentally.

In the present study, we paid attention to Co_2MnAl , which is another interesting material predicted to show large intrinsic anomalous Hall effect (AHE) [22,23] due to the existence of Weyl points near E_F [24]. Previous experiments claimed the observation of large AHE in the Co_2MnAl film having a random disordering between Mn and Al, so-called $B2$ disorder [Figs. 1(a) and 1(b)] [25]. However, they showed only anomalous Hall resistivity ρ_{xy} as evidence of large AHE

*Corresponding author: SAKURABA.Yuya@nims.go.jp

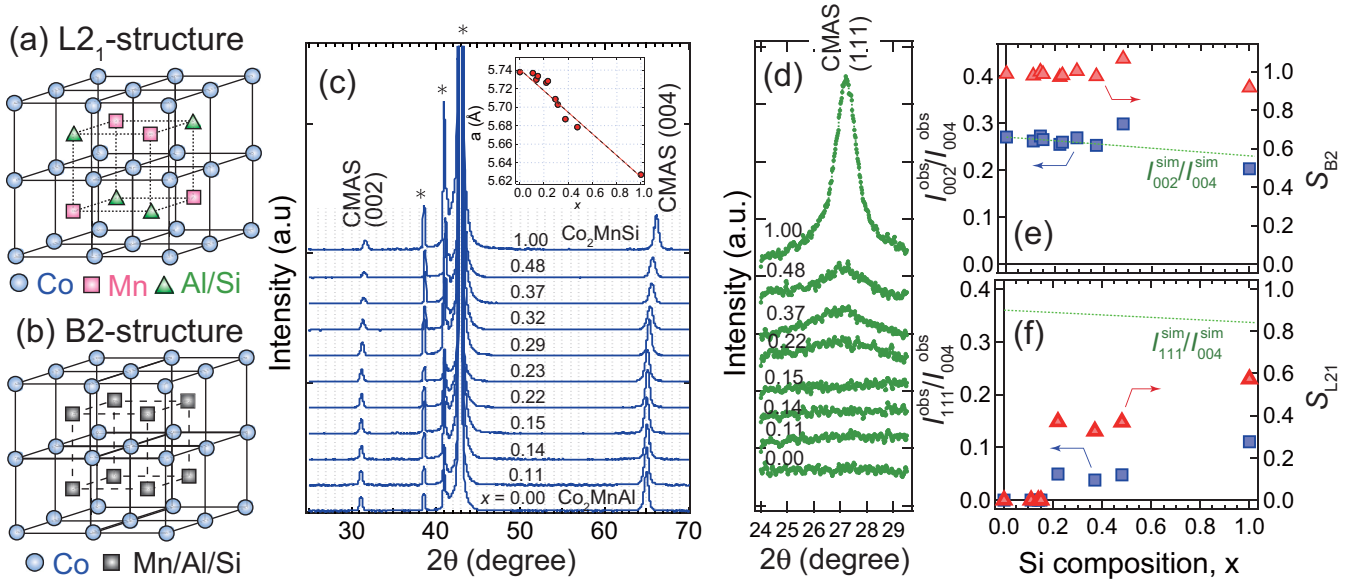


FIG. 1. (a, b) Schematic views of $L2_1$ and $B2$ structure of CMAS. (c) Out-of-plane XRD patterns for $\text{Co}_2\text{MnAl}_{1-x}\text{Si}_x$ thin films annealed at 600°C . The peaks denoted by * originate from MgO (001) substrate. The inset shows Si composition x dependence of lattice constant a evaluated from position of (004) peak position. (d) XRD patterns measured by tilting the film normal plane by 54.7° to see the (111) superlattice peak. (e, f) The x dependence of $I_{002}^{\text{obs}}/I_{004}^{\text{obs}}$, $I_{111}^{\text{obs}}/I_{004}^{\text{obs}}$, S_{B2} , and S_{L21} evaluated by Eqs. (2) and (3), respectively.

and did not compare anomalous Hall conductivity σ_{xy} with the theoretical value, although σ_{xy} is the intrinsic physical parameter that is theoretically accessible [26,27]. Therefore, strictly speaking, the theoretically predicted large AHE has never been confirmed in Co_2MnAl . It is well known that it is not easy to form $L2_1$ ordering in Co_2MnAl , especially in thin film [25,28]. Co_2MnAl often has $B2$ ordering in which Mn and Al atoms are randomly disordered because of too small driving force to form $L2_1$, as indicated by very low $L2_1$ to $B2$ order-disorder transition temperature $T_i^{L2_1/B2}$ of 950 K [29], which is much lower than $T_i^{L2_1/B2}$ in Co_2MnGa , 1200 K. It is expected that the atomic ordering in Co_2MnAl can be largely improved by the replacement of Al with Si, because $L2_1$ - Co_2MnSi is the thermally stable intermetallic ordered compound that keeps the $L2_1$ ordered structure up to its melting temperature ~ 1400 K, namely, $T_i^{L2_1/B2}$ was estimated to be 1580 K [30], which is higher than its melting point. In addition, previous study revealed that the position of E_F in Co_2MnAl can be tuned toward higher energy by substituting Si with Al [31,32]. Therefore, $\text{Co}_2\text{MnAl}_{1-x}\text{Si}_x$ is a suitable material to investigate how the position of Weyl points against E_F and atomic ordering influences AHE and ANE.

II. EXPERIMENTAL AND CALCULATION METHODS

(001)-oriented epitaxial $\text{Co}_2\text{MnAl}_{1-x}\text{Si}_x$ (CMAS) thin films having different Si:Al ratios were grown on a MgO (001) substrate using a cosputtering technique with Co_2MnSi and Co_2MnAl sputtering targets. All films were deposited at ambient substrate temperature and then in situ annealed at 600°C . The composition of the films was measured by a combination of inductively coupled plasma mass

spectrometry (ICP-MS) and x-ray fluorescence analysis (XRF). In this study we made eleven CMAS thin films having a different Si:Al composition ratio x . The compositions of two CMAS films having nominal $x = 0$ and 0.25 were measured by inductively coupled plasma mass spectrometry (ICP-MS) and determined to be nearly stoichiometric $\text{Co}_{1.93}\text{Mn}_{0.98}\text{Al}_{1.08}$ and $\text{Co}_{1.88}\text{Mn}_{0.95}\text{Al}_{0.90}\text{Si}_{0.27}$ in at %, respectively. Although we found a slight off stoichiometry of Co and Mn compositions, we focus on the effect of Si:Al ratio x on various properties in this study. Thus the x for all CMAS films is evaluated by XRF to be 0.00, 0.11, 0.14, 0.15, 0.22, 0.23, 0.29, 0.32, 0.37, 0.48, and 1.00. For simplification, we express each CMAS film in “ $\text{Co}_2\text{MnAl}_{1-x}\text{Si}_x$ ” using x measured by XRF. The annealing temperature T_{ann} dependence was studied for the films with $x = 0$ and 0.37 from 500 to 700°C to investigate the atomic ordering effect on ANE. The thickness of the films was fixed at 30 nm. The crystal structure and atomic ordering were investigated by x-ray diffraction with a Cu $K\alpha$ source. Longitudinal and transverse electric and thermoelectric transport properties, including ANE, were investigated with a physical property measurement system (PPMS) for the films patterned by photolithography and Ar ion milling. The electric resistivity ρ_{xx} was measured using a dc four-probe method by flowing a constant dc current of 1 mA. ANE (AHE) was measured by flowing a heat (electric) current in the film plane direction and applying a magnetic field in the perpendicular direction in the PPMS at 300 K. As for ANE, the temperature gradient ∇T in PPMS was carefully evaluated through the following procedure: First ∇T outside of the PPMS was measured using an infrared (IR) camera (InfReC R450, Nippon Avionics) for the sample with black body coating to correct the emissivity of the samples. At the same time, the Seebeck voltage V_{SE}

in the film was measured outside, then the linear relationship between V_{SE} and ∇T was obtained. After that, ANE voltage V_{ANE} was measured together with V_{SE} in PPMS; then ∇T in PPMS can be estimated through the V_{SE} . The same technique has been utilized in previous studies [3,20]. To improve the quantitative reliability of the observed ∇T in this study, we measured the given ∇T by the patterned on-chip thermometer that was employed in Ref. [18], for one of the CMAS films and gave a calibration to ∇T measured by the method using an IR camera (see the Supplemental Material for details [33]). For a strict evaluation of the Seebeck coefficient S_{SE} , we used a Seebeck coefficient/electric resistance measurement system (ZEM-3, Advance Riko, Inc.). We also performed a first-principles calculation to evaluate σ_{xy} . The first-principles technique was the tight-binding linearized muffin-tin orbital method under the local spin-density approximation [34]. To consider the AHE effect, the spin-orbital-coupling term under the Pauli approximation was added to the nonrelativistic Hamiltonian. σ_{xy} was calculated from the Kubo-Bastin formula consisting of Fermi surface and Fermi sea terms [35]. Since previous theoretical studies have calculated σ_{xy} in only ideal L_{21} -ordered cases [22,23], in this study the electron scattering effect originating from $B2$ disorder on σ_{xy} was taken into account in the coherent-potential approximation [34] with our own developed scheme of the calculation [36]. About 5×10^7 k points were used for the Fermi surface term and from 1×10^6 to 5×10^7 , depending on the energy variable in the integration for the Fermi sea term in the full Brillouin zone [35].

III. RESULTS AND DISCUSSION

A. Structural analysis in $\text{Co}_2\text{MnAl}_{1-x}\text{Si}_x$ films

Out-of-plane x-ray diffraction (XRD) patterns for the CMAS films annealed at 600 °C are shown in Fig. 1(c). We clearly detected only (002) and (004) peaks from all CMAS films, indicating (001)-oriented growth in the whole range of x . A clear (002) superlattice peak indicates the existence of atomic ordering between Co and (Mn,Al/Si) sites, so-called $B2$ structure [Fig. 1(b)]. The out-of-plane lattice constant a , as evaluated from the (004) peak position, is plotted versus x in the inset of Fig. 1(c). The a values for Co_2MnAl and Co_2MnSi films are 5.74 and 5.63 Å, respectively, which is similar with the reported values in literature, 5.755 and 5.654 Å [30]. The a almost linearly decreases with increasing Si composition ratio, following Vegard's law, indicating a formation of single-phase CMAS in the whole range of x . We also measured the (111) superlattice peak arising from the L_{21} -ordered structure by tilting the film plane to 54.7° from the normal direction. No (111) peak appears from $x = 0$ to 0.15, but a tiny detectable peak is observed from $x = 0.22$ to 0.48, as shown in Fig. 1(d). The (111) peak intensity appears to be larger with increasing Si composition ratio, and the strongest peak was observed in Co_2MnSi , which can be explained by enlargement of $T_i^{L_{21}/B_2}$ by the substitution of Si with Al in Co_2MnAl , as mentioned earlier. For evaluating the degree of $B2$ and L_{21} ordering, S_{B2} and $S_{L_{21}}$, we performed the XRD pattern simulation for L_{21} -ordered Co_2MnAl and Co_2MnSi using visualization for electronic and structural analysis

(VESTA) and then calculated S_{B2} and $S_{L_{21}}$ using the following equations:

$$S_{B2}^2 = \frac{I_{002}^{\text{obs}}/I_{004}^{\text{obs}}}{I_{002}^{\text{sim}}/I_{004}^{\text{sim}}}, \quad (2)$$

$$S_{L_{21}}^2 = \frac{I_{111}^{\text{obs}}/I_{004}^{\text{obs}}}{I_{111}^{\text{sim}}/I_{004}^{\text{sim}}}. \quad (3)$$

Here I_{hkl}^{sim} is the simulated (hkl) peak intensity after giving a correction by considering the multiplicity factor, absorption factor, and Lorentz polarization factor. I_{hkl}^{obs} is the integrated peak intensity for the experimentally observed (hkl) peak. The x dependence of $I_{002}^{\text{obs}}/I_{004}^{\text{obs}}$, $I_{111}^{\text{obs}}/I_{004}^{\text{obs}}$, S_{B2} , and $S_{L_{21}}$ are summarized in Figs. 1(e) and 1(f). We confirmed that degree of S_{B2} is nearly 1 in the whole range of x , indicating nearly perfect $B2$ ordering exists in these CMAS films. In contrast, $S_{L_{21}}$ is much smaller than 1; $S_{L_{21}} = 0$ from $x = 0$ to 0.15, 0.32–0.37 from $x = 0.22$ to 0.48, and 0.57 for $x = 1$. This imperfection of L_{21} ordering affects the AHE and ANE as discussed later.

A recent study clearly found that the sign of anisotropic magnetoresistance (AMR) in Co-based Heusler is sensitive to the position of E_F inside/outside the energy gap in the minority spin channel (half-metallic gap), namely, the sign of AMR is negative (positive) when E_F is inside (outside) of the half-metallic gap [32,37,38]. Therefore we measured AMR for our CMAS films to see the change of E_F position indirectly and found the clear sign change from positive to negative from CMA to CMS at around $x = 0.4$ (see Supplemental Material [39]). This result supports the E_F shifting toward higher energy by replacing Si with Al as we expected.

B. Anomalous Hall effect in $\text{Co}_2\text{MnAl}_{1-x}\text{Si}_x$ films

Figure 2(a) shows the perpendicular magnetic field dependence of the anomalous Hall resistivity ρ_{yx} for the CMAS thin films measured at 300 K. The Co_2MnAl film had the largest ρ_{yx} of about +18 $\mu\Omega$ cm, which is a very close value with the previous study [25]. ρ_{yx} almost monotonically decreases upon replacing Al with Si, as shown in Fig. 2(b), and the Co_2MnSi film had the smallest ρ_{yx} , 0.7 $\mu\Omega$ cm. This result well agrees with the previous study of Hall effect in $\text{Co}_2\text{MnSi}_{1-x}\text{Al}_x$ polycrystalline bulk samples reported by Prestigiacomo *et al.* [40]. The longitudinal conductivity ρ_{xx} shown in Fig. 2(b) is nearly constant at about 240–260 $\mu\Omega$ cm in the region of $x = 0$ –0.32, and then reduces down to 83 $\mu\Omega$ cm from 0.37 to 1.00, which seems to be related with the improvement of L_{21} ordering with Si. The anomalous Hall angle θ_{AHE} and anomalous Hall conductivity σ_{xy} are evaluated using the equations $\theta_{\text{AHE}} = \rho_{yx}/\rho_{xx}$ and $\sigma_{xy} = \rho_{yx}/(\rho_{xx}^2 + \rho_{yx}^2)$, respectively, and plotted in Figs. 2(d) and 2(e). θ_{AHE} clearly monotonically decreases with increasing Si; Co_2MnAl showed the largest magnitude of anomalous Hall angle, $|\theta_{\text{AHE}}|$ of 7.3%, whereas $|\theta_{\text{AHE}}|$ decreases with x to 0.8% in Co_2MnSi . It should be noted here that the σ_{xy} obtained for Co_2MnAl and Co_2MnSi are 295 (362) and 96 (101) S/cm at 300 K (10 K), respectively, which are lower than the calculated intrinsic contribution of AHE, σ_{xy}^{int} , 1265 and 193 S/cm for L_{21} -ordered Co_2MnAl and Co_2MnSi

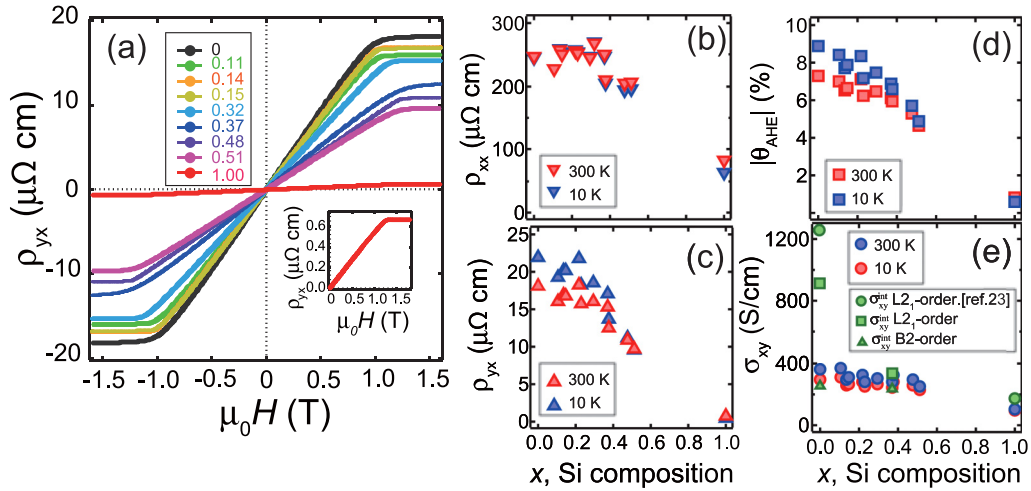


FIG. 2. (a) Perpendicular magnetic field H dependence of anomalous Hall resistivity ρ_{xx} for $\text{Co}_2\text{MnAl}_{1-x}\text{Si}_x$ thin films measured at 300 K. Si composition dependence of ρ_{xx} . Inset magnified the data for Co_2MnSi (b), ρ_{yx} (c), anomalous Hall angle $|\theta_{\text{AHE}}|$ (d), and σ_{xy} (e). The data measured at 10 and 300 K are shown in (b–e). Theoretical σ_{xy}^{int} for $L2_1$ - and $B2$ - Co_2MnAl and $\text{Co}_2\text{MnAl}_{0.63}\text{Si}_{0.37}$ are also plotted in (e).

[23]. Since the theoretical intrinsic mechanism contribution for AHE does not take any electron scattering effect into consideration, experimentally observed σ_{xy} in thin films is reduced even at low temperature by unavoidable scatterings at the surface/interface such as the film surface, film/substrate interface, and grain boundaries. As the σ_{xy} in Fe epitaxial film reduces with decreasing its thickness [41], the existence of electron scattering can be one reason for $\sigma_{xy} < \sigma_{xy}^{\text{int}}$. However, the deviation between σ_{xy} and σ_{xy}^{int} for Co_2MnAl seems too large [see Fig. 2(e)] to be explained by such an additional scattering. To understand this mechanism, we calculated the density of states (DOS) and σ_{xy}^{int} for not only $L2_1$ and but also $B2$ Co_2MnAl [Figs. 3(a) and 3(c)]. As shown in Fig. 3(c), calculated σ_{xy}^{int} in $L2_1$ - Co_2MnAl exhibits large variation from 300 to 1600 S/cm within even a small ± 0.3 eV range around E_F and takes a large value of 931 S/cm at E_F . On the other hand, disordered $B2$ - Co_2MnAl was predicted to show much smaller σ_{xy}^{int} , 258 S/cm, at E_F with small slope against energy. As shown in Fig. 2(e), this σ_{xy}^{int} for $B2$ - Co_2MnAl is close

to the experimental σ_{xy} . Although it has not been elucidated by our calculation how Berry curvature in the momentum space changes from $L2_1$ to $B2$ disordering structures, it is expected the $B2$ disorder smears the whole band dispersion, including the bands forming the Weyl points, which is expected to reduce the Berry curvature near the Fermi level. This smearing effect of band dispersion can be seen from the blurred total DOS of $B2$ structure compared to the sharp DOS of $L2_1$, as shown in Figs. 3(a) and 3(c). Thus, it is concluded that observed small σ_{xy} in $B2$ - Co_2MnAl film is attributed to this intrinsic reduction of σ_{xy}^{int} from $L2_1$ to $B2$. To see the Si substitution effect, we also calculated DOS and σ_{xy}^{int} for $L2_1$ and $B2$ $\text{Co}_2\text{MnAl}_{0.63}\text{Si}_{0.37}$ as shown in Figs. 3(b) and 3(d), respectively. If one compares the DOS in $L2_1$ -ordered $\text{Co}_2\text{MnAl}_{0.63}\text{Si}_{0.37}$ with that in Co_2MnAl , it is clearly confirmed that the E_F shifts by about +0.2 eV with keeping the shape of DOS near E_F . Because of this shift of E_F , the peak of σ_{xy}^{int} we can see near E_F in $L2_1$ - Co_2MnAl appears at around -0.22 eV in $\text{Co}_2\text{MnAl}_{0.63}\text{Si}_{0.37}$. Consequently, we can see a small difference of σ_{xy}^{int} between $L2_1$ and $B2$, 370 and 268 S/cm, in $\text{Co}_2\text{MnAl}_{0.63}\text{Si}_{0.37}$, which can be an explanation for the observed small σ_{xy} in the $\text{Co}_2\text{MnAl}_{0.63}\text{Si}_{0.37}$ film and other CMAS films of $x = 0.22$ – 0.51 , regardless of their partial $L2_1$ ordering.

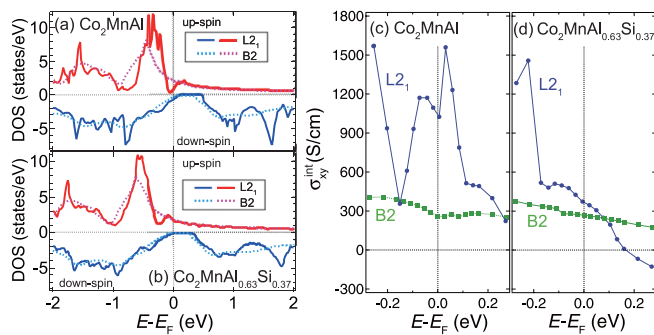


FIG. 3. First-principles calculation of the spin-resolved DOS for (a) Co_2MnAl and (b) $\text{Co}_2\text{MnAl}_{0.63}\text{Si}_{0.37}$ in Figs. 3(b) and 3(d). For both compositions we calculated the DOS in $L2_1$ and $B2$ structure. Calculated energy dependence of σ_{xy} for $B2$ and $L2_1$ -ordered (c) Co_2MnAl and (d) $\text{Co}_2\text{MnAl}_{0.63}\text{Si}_{0.37}$.

C. Anomalous Nernst effect in $\text{Co}_2\text{MnAl}_{1-x}\text{Si}_x$ films

The x dependence of thermopower of ANE and Seebeck effect (S_{ANE} and S_{SE} , respectively) are summarized in Figs. 4(a) and 4(b). Interestingly, the Co_2MnAl film that showed the largest AHE exhibits a small S_{ANE} of $+0.9 \mu\text{V}/\text{K}$, and S_{ANE} gradually grows as more Al is substituted with Si. The largest S_{ANE} of $+3.6 \mu\text{V}/\text{K}$ was observed for $\text{Co}_2\text{MnAl}_{0.63}\text{Si}_{0.37}$. Above $x = 0.37$ the S_{ANE} reduces with following x , finally dropping down to $+0.7 \mu\text{V}/\text{K}$ for Co_2MnSi . On the other hand, the sign of S_{SE} is negative in the whole range of x . With increasing x , the magnitude of S_{SE} gradually increases with x from $-7.7 \mu\text{V}/\text{K}$ in Co_2MnAl to $-21.1 \mu\text{V}/\text{K}$

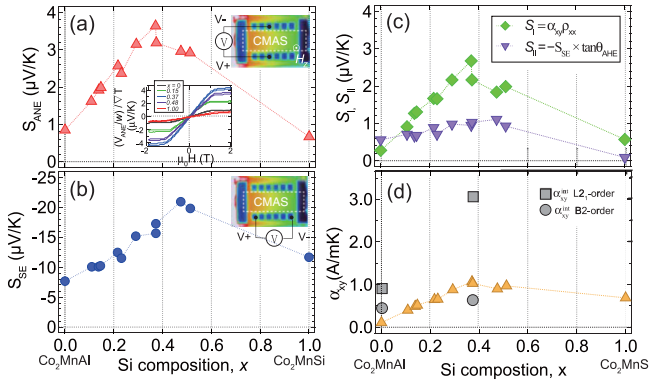


FIG. 4. Si composition x dependence of S_{ANE} (a), S_{SE} (b), S_I (c), and α_{xy} (d). The inset of (b) shows the external magnetic field dependence of V_{ANE} normalized by the sample width w and given temperature gradient ∇T in CMAS films. Theoretically calculated α_{xy}^{int} using Eq. (5) are also plotted in (d).

in $\text{Co}_2\text{MnAl}_{0.52}\text{Si}_{0.48}$, then decreases to $-11.7 \mu\text{V/K}$ in Co_2MnSi . Therefore, we found that the x for the highest AHE, Seebeck effect, and ANE are different in prepared CMAS films. Here we analyze the ANE in CMAS using the following linear response equation of S_{ANE} :

$$S_{ANE} = \rho_{xx}\alpha_{xy} + \rho_{xy}\alpha_{xx}. \quad (4)$$

Here α_{xx} and α_{xy} are the longitudinal and transverse Peltier coefficient, respectively. Equation (4) tells us that there are two different origins in ANE. For simplifying the following explanation, we denote the first and second terms as $S_I = \rho_{xx}\alpha_{xy}$ and $S_{II} = \rho_{xy}\alpha_{xx}$, respectively. Since $S_{SE} = \rho_{xx}\alpha_{xx}$, S_{II} can be converted to $-S_{SE}\tan\theta_{AHE}$; therefore, S_{II} is regarded as the contribution of AHE on ANE induced by a Seebeck-driven longitudinal current. On the other hand, S_I originates from the direct conversion of the temperature gradient to transverse current via α_{xy} as expressed in $\alpha_{xy}\nabla T = i_{xy}$. Figure 4(c) plots S_{II} estimated from observed S_{SE} and θ_{AHE} versus x . Although we observed a large difference of x dependence between the magnitudes of AHE and ANE in the CMAS films, the trend of x dependence of S_{II} is similar to that of S_{ANE} . An important point here is that the magnitude of S_{II} is smaller than the observed S_{ANE} in the entire range of x . Thus the remaining part of S_{ANE} would arise from S_I by following Eq. (4). The evaluated S_I is also plotted in Fig. 4(c). It can be seen that the contribution of S_I is larger than S_{II} except for Co_2MnAl . Particularly, the largest S_{ANE} of $+3.6 \mu\text{V/K}$ at $x = 0.37$ arises from the constructive but dominant contribution of S_I ($+2.7 \mu\text{V/K}$) against S_{II} ($+0.9 \mu\text{V/K}$). α_{xy} evaluated from $\alpha_{xy} = S_I/\rho_{xx}$ is plotted in Fig. 4(d). It is clearly seen that α_{xy} becomes larger by replacing more Al with Si, indicating that α_{xy} is sensitive to the position of the Fermi level and atomic ordering. The α_{xy} for Co_2MnAl and $\text{Co}_2\text{MnAl}_{0.63}\text{Si}_{0.37}$ films are 0.11 and 1.07 A/mK, respectively. α_{xy} originating from the intrinsic contribution of AHE, α_{xy}^{int} , can be theoretically evaluated from the energy dependence of σ_{xy}^{int} using the following Mott's relation based on the classic Boltzmann equation [42]:

$$\alpha_{xy}^{int} = \frac{1}{-eT} \int_{-\infty}^{\infty} \sigma_{xy}^{int}(\varepsilon)(\varepsilon - E_F) \left(-\frac{df}{d\varepsilon} \right) d\varepsilon. \quad (5)$$

To obtain α_{xy}^{int} at 300 K, we calculated α_{xy}^{int} by setting $\pm 260 \text{ meV} (= 0.02 \text{ Ry})$ as the integration range of this calculation, which is large enough to consider the major contribution of $\frac{df}{d\varepsilon}(\varepsilon, T)$ around E_F at 300 K. As shown in Fig. 4(d), calculated α_{xy}^{int} for L_{21} and $B2$ - $\text{Co}_2\text{MnAl}(\text{Co}_2\text{MnAl}_{0.63}\text{Si}_{0.37})$ are 0.92 (3.08) and 0.47 (0.57), respectively. Simply speaking, α_{xy}^{int} is sensitive to the shape and slope of σ_{xy}^{int} at around E_F , namely, even (odd) functionlike behavior leads to small (large) α_{xy}^{int} . As we can see in Fig. 3(c), L_{21} - Co_2MnAl shows nearly even functionlike behavior around E_F within the integration range, whereas, L_{21} - $\text{Co}_2\text{MnAl}_{0.63}\text{Si}_{0.37}$ shows odd functionlike behavior with a large negative slope, which is a reason for much larger α_{xy}^{int} in L_{21} - $\text{Co}_2\text{MnAl}_{0.63}\text{Si}_{0.37}$. In the $B2$ disordered case, because σ_{xy}^{int} shows a very small change in both Co_2MnAl and $\text{Co}_2\text{MnAl}_{0.63}\text{Si}_{0.37}$, α_{xy}^{int} was estimated to be very small. As can be seen in Fig. 4(d), experimental α_{xy} for $\text{Co}_2\text{MnAl}_{0.63}\text{Si}_{0.37}$ is close to the calculated value for the $B2$ case but is reasonably located in between L_{21} and $B2$. Therefore, we concluded that the enlargement of α_{xy} in our CMAS thin films is attributed to not only Fermi level shifting but also the improvement of L_{21} atomic ordering by Si substitution for Al.

To see the effect of atomic ordering more clearly, we investigated the annealing temperature dependence T_{ann} of atomic ordering, AHE and ANE in the Co_2MnAl and $\text{Co}_2\text{MnAl}_{0.63}\text{Si}_{0.37}$ films. Figure 5(a) shows the T_{ann} dependence of the degree of L_{21} ordering $S_{L_{21}}$ evaluated by Eq. (3). Co_2MnAl film does not show a (111) peak even after annealing at 700°C , indicating that Co_2MnAl film keeps the $B2$ disordered structure regardless of T_{ann} . Therefore, σ_{xy} in Co_2MnAl film is around 300 S/cm and shows no remarkable variation against T_{ann} [Fig. 5(b)]. In contrast, tiny (111) that appears at $T_{ann} = 600^\circ\text{C}$ in $\text{Co}_2\text{MnAl}_{0.63}\text{Si}_{0.37}$ was strongly enlarged by increasing T_{ann} up to 650°C . $S_{L_{21}}$ increases from 0.32 at 600°C to 0.66 at 650°C . Oppositely, the (111) peak does not appear at 500°C . Observed σ_{xy} in $\text{Co}_2\text{MnAl}_{0.63}\text{Si}_{0.37}$ gradually increases with T_{ann} [Fig. 5(b)] from 136 S/cm at 500°C to 275 S/cm at 700°C , whose tendency is in qualitative agreement with the variation of the calculated σ_{xy}^{int} from $B2$ to L_{21} structure shown in Fig. 3(d). A drastic increase of S_{SE} and S_{ANE} were also observed in the $\text{Co}_2\text{MnAl}_{0.63}\text{Si}_{0.37}$ annealed above 650°C [Figs. 5(c), 5(d) and 5(e)], in contrast to no remarkable change in the Co_2MnAl versus T_{ann} , indicating that the enlargement of both S_{SE} and S_{ANE} arises from the improvement of L_{21} ordering. The highest S_{ANE} of $5.7 \mu\text{V/K}$, which is comparable to the previous reports in Co_2MnGa [7,8], was observed for the $\text{Co}_2\text{MnAl}_{0.63}\text{Si}_{0.37}$ film annealed at 650°C . At the same time, as can be seen in Fig. 5(f), α_{xy} reaches 1.68 A/mK at 650°C , which is located in between theoretical α_{xy}^{int} for L_{21} and $B2$, as expected from the evaluated imperfect $S_{L_{21}}$. Such large α_{xy} gives rise to dominant S_I contribution of $4.0 \mu\text{V/K}$ for the total ANE of $5.7 \mu\text{V/K}$. Therefore, it is suggested that giant ANE in CMAS film achieved in this study is due to both the Fermi level shifting and improvement of L_{21} atomic ordering in Co_2MnAl . We should note that because our CMAS films do not have ideal L_{21} ordering, higher ANE might be possible by improving the degree of L_{21} ordering.

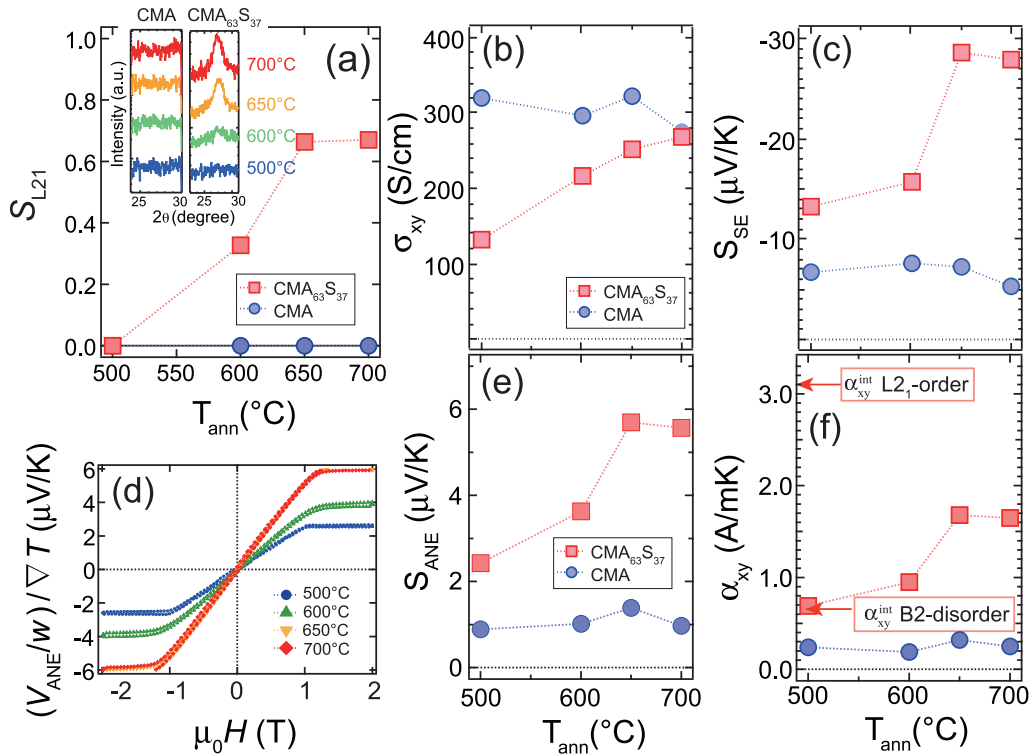


FIG. 5. (a) T_{ann} dependence of S_{L21} in Co_2MnAl and $\text{Co}_2\text{MnAl}_{0.63}\text{Si}_{0.37}$ films. Inset shows XRD patterns in Co_2MnAl and $\text{Co}_2\text{MnAl}_{0.63}\text{Si}_{0.37}$ thin films in the 2θ range of (111) peak. T_{ann} dependence of σ_{xy} , S_{SE} , S_{ANE} , and α_{xy} in Co_2MnAl and $\text{Co}_2\text{MnAl}_{0.63}\text{Si}_{0.37}$ are shown in (b), (c), (e), and (f), respectively. The arrows in (f) are the theoretical α_{xy}^{int} for $L2_1$ and $B2$ $\text{Co}_2\text{MnAl}_{0.63}\text{Si}_{0.37}$. (d) External magnetic field dependence of V_{ANE} normalized by the sample width w and given temperature gradient ∇T in $\text{Co}_2\text{MnAl}_{0.63}\text{Si}_{0.37}$ annealed at different temperature.

IV. CONCLUSIONS

In conclusion, in this work we studied anomalous Hall and Nernst effects in $\text{Co}_2\text{MnAl}_{1-x}\text{Si}_x$ from both experiment and first-principles calculation to see the effect of Fermi level position and the degree of atomic ordering on AHE and ANE. It was clearly confirmed that Fermi level shifts toward higher energy and $L2_1$ ordering improves with increasing Si composition ratio x . Observed σ_{xy} in the Co_2MnAl film having no $L2_1$ ordering is much smaller than the calculated intrinsic σ_{xy} for $L2_1$ -order structure but close to our calculation for a $B2$ -disordered structure, suggesting that theoretically predicted large AHE due to the existence of Weyl points in Co_2MnAl is weakened by $B2$ disordering in reality. Although Al substitution with Si does not strongly affect σ_{xy} , the transverse Peltier coefficient α_{xy} was clearly enlarged with increasing Si, and the highest α_{xy} was obtained in $\text{Co}_2\text{MnAl}_{0.63}\text{Si}_{0.37}$. As predicted by our calculation, α_{xy} was enlarged by improving $L2_1$ ordering in $\text{Co}_2\text{MnAl}_{0.63}\text{Si}_{0.37}$, and finally, a giant ANE

thermopower of $5.7 \mu\text{V}/\text{K}$ was achieved in $\text{Co}_2\text{MnAl}_{0.63}\text{Si}_{0.37}$ film having a mixture of $L2_1$ and $B2$ phase. Our result indicates that both Fermi level tuning and high atomic ordering is critically important to realize exotic transverse transports in Co-based Heusler Weyl semimetals. This knowledge will be beneficial for future material development to realize practical thermoelectric applications using ANE.

ACKNOWLEDGMENTS

The authors thank K. Masuda, K. Sumida, A. Kimura, W. Zhou, K. Takanashi, S. Maekawa, E. Saitoh, K. Hono, and K. Uchida for valuable discussions, and N. Kojima, H. Ikeda, and B. Masaoka for various technical supports. This work was supported by a JSPS KAKENHI Grant-in-Aid for Young Scientists (A) (No. JP26709045), PRESTO from the Japan Science and Technology Agency (No. JPMJPR17R5), and NEDO.

- [1] Y. Sakuraba, K. Hasegawa, M. Mizuguchi, T. Kubota, S. Mizukami, T. Miyazaki, and K. Takanashi, *Appl. Phys. Express* **6**, 033003 (2013).
- [2] Y. Sakuraba, *Scr. Mater.* **111**, 29 (2016).
- [3] W. Zhou and Y. Sakuraba, *Appl. Phys. Express* **13**, 043001 (2020).

- [4] M. Ikhlas, T. Tomita, T. Koretsune, M.-T. Suzuki, D. Nishio-Hamane, R. Arita, Y. Otani, and S. Nakatsuji, *Nat. Phys.* **13**, 1085 (2017).
- [5] K. Hasegawa, M. Mizuguchi, Y. Sakuraba, T. Kamada, T. Kojima, T. Kubota, S. Mizukami, T. Miyazaki, and K. Takanashi, *Appl. Phys. Lett.* **106**, 252405 (2015).

- [6] G. Chang, S.-Y. Xu, X. Zhou, S.-M. Huang, B. Singh, B. Wang, I. Belopolski, J. Yin, S. Zhang, A. Bansil, H. Lin, and M. Zahid Hasan, *Phys. Rev. Lett.* **119**, 156401 (2017).
- [7] A. Sakai, Y. P. Mizuta, A. Agung Nugroho, R. Sihombing, T. Koretsune, M.-T. Suzuki, N. Takemori, R. Ishii, D. Nishio-Hamane, R. Arita, P. Goswami, and S. Nakatsuji, *Nat. Phys.* **14**, 1119 (2018).
- [8] S. N. Guin, K. Manna, J. Noky, S. J. Watzman, C. Fu, N. Kumar, W. Schnelle, C. Shekhar, Y. Sun, J. Gooth, and C. Felser, *NPG Asia Mater.* **11**, 16 (2019).
- [9] I. Belopolski, K. Manna, D. S. Sanchez, G. Chang, B. Ernst, J. Yin, S. S. Zhang, T. Cochran, N. Shumiya, H. Zheng, B. Singh, G. Bian, D. Multer, M. Litskevich, X. Zhou, S. M. Huang, B. Wang, T. R. Chang, S.Y. Xu, A. Bansil, C. Felser, H. Lin, and M. Zahid Hasan, *Science* **365**, 1278 (2019).
- [10] K. I. Uchida, T. Kikkawa, T. Seki, T. Oyake, J. Shiomi, Z. Qiu, K. Takanashi, and E. Saitoh, *Phys. Rev. B* **92**, 094414 (2015).
- [11] Y. P. Mizuta and F. Ishii, *Sci. Rep.* **6**, 28076 (2016).
- [12] D. J. Kim, K. D. Lee, S. Surabhi, S. G. Yoon, J. R. Jeong, and B. G. Park, *Adv. Funct. Mater.* **26**, 5507 (2016).
- [13] H. Narita, M. Ikhlās, M. Kimata, A. A. Nugroho, S. Nakatsuji, and Y. Otani, *Appl. Phys. Lett.* **111**, 202404 (2017).
- [14] S. Tu, J. Hu, G. Yu, H. Yu, C. Liu, F. Heimbach, X. Wang, J. Zhang, Y. Zhang, A. Hamzić, K. L. Wang, W. Zhao, and J.-P. Ansermet, *Appl. Phys. Lett.* **111**, 222401 (2017).
- [15] T. C. Chuang, P. L. Su, P. H. Wu, and S. Y. Huang, *Phys. Rev. B* **96**, 174406 (2017).
- [16] Z. Yang, E. A. Codecido, J. Marquez, Y. Zheng, J. P. Heremans, and R. C. Myers, *AIP Adv.* **7**, 095017 (2017).
- [17] S. Isogami, K. Takanashi, and M. Mizuguchi, *Appl. Phys. Express* **10**, 073005 (2017).
- [18] H. Reichlova, R. Schlitz, S. Beckert, P. Swekis, A. Markou, Y.-C. Chen, D. Kriegner, S. Fabretti, G. H. Park, A. Niemann, S. Sudheendra, A. Thomas, K. Nielsch, C. Felser, and S. T. B. Goennenwein, *Appl. Phys. Lett.* **113**, 212405 (2018).
- [19] A. Miura, H. Sepelri-Amin, K. Masuda, H. Tsuchiura, Y. Miura, R. Iguchi, Y. Sakuraba, J. Shiomi, K. Hono and K.-i. Uchida, *Appl. Phys. Lett.* **115**, 222403 (2019).
- [20] H. Nakayama, K. Masuda, J. Wang, A. Miura, K.-i. Uchida, M. Murata, and Y. Sakuraba, *Phys. Rev. Mater.* **3**, 114412 (2019).
- [21] T. Miyasato, N. Abe, T. Fujii, A. Asamitsu, S. Onoda, Y. Onose, N. Nagaosa, and Y. Tokura, *Phys. Rev. Lett.* **99**, 086602 (2007).
- [22] J. Kübler and C. Felser, *Phys. Rev. B* **85**, 012405 (2012).
- [23] J. C. Tung and G. Y. Guo, *New J. Phys.* **15**, 033014 (2013).
- [24] J. Kübler and C. Felser, *EPL* **114**, 47005 (2016).
- [25] E. Vilanova Vidal, G. Stryganyuk, H. Schneider, C. Felser, and G. Jakob, *Appl. Phys. Lett.* **99**, 132509 (2011).
- [26] Y. Yao, L. Kleinman, A. H. MacDonald, J. Sinova, T. Jungwirth, D. Wang, E. Wang, and Q. Niu, *Phys. Rev. Lett.* **92**, 037204 (2004).
- [27] N. Nagaosa, J. Sinova, S. Onoda, A. H. MacDonald, and N. P. Ong, *Rev. Mod. Phys.* **82**, 1539 (2010).
- [28] Y. Sakuraba, J. Nakata, M. Oogane, H. Kubota, Y. Ando, A. Sakuma, and T. Miyazaki, *Jpn. J. Appl. Phys., Part 1* **44**, 6535 (2005).
- [29] T. Nakatani, S. Li, Y. Sakuraba, T. Furubayashi, and K. Hono, *IEEE Trans. Magn.* **54**, 3300211 (2017).
- [30] R. Y. Umetsu, K. Kobayashi, A. Fujita, R. Kainuma, and K. Ishida, *Scr. Mater.* **58**, 723 (2008).
- [31] Y. Sakuraba, K. Takanashi, Y. Kota, T. Kubota, M. Oogane, A. Sakuma, and Y. Ando, *Phys. Rev. B* **81**, 144422 (2010).
- [32] Y. Sakuraba, S. Kokado, Y. Hirayama, T. Furubayashi, H. Sukegawa, S. Li, Y. K. Takahashi, and K. Hono, *Appl. Phys. Lett.* **104**, 172407 (2014).
- [33] See Supplemental Material at <http://link.aps.org/supplemental/10.1103/PhysRevB.101.134407> for the detail of the evaluation method of ∇T using the on-chip thermometer.
- [34] I. Turek, *Electronic Structure of Disordered Alloys, Surfaces and Interfaces*, 1997 ed. (Springer, Berlin, 1996).
- [35] I. Turek, J. Kudrnovský, and V. Drchal, *Phys. Rev. B* **89**, 064405 (2014).
- [36] K. Hyodo, A. Sakuma, and Y. Kota, *Phys. Rev. B* **94**, 104404 (2016).
- [37] F. J. Yang, Y. Sakuraba, S. Kokado, Y. Kota, A. Sakuma, and K. Takanashi, *Phys. Rev. B* **86**, 020409(R) (2012).
- [38] S. Kokado, M. Tsunoda, K. Harigaya, and A. Sakuma, *J. Phys. Soc. Japan* **81**, 24705 (2012).
- [39] See Supplemental Material at <http://link.aps.org/supplemental/10.1103/PhysRevB.101.134407> for the detail of the CMAS composition dependence of the AMR ratio.
- [40] J. C. Prestigiacomo, D. P. Young, P. W. Adams, and S. Stadler, *J. Appl. Phys.* **115**, 043712 (2014).
- [41] S. Sangiao, L. Morellon, G. Simon, J. M. De Teresa, J. A. Pardo, J. Arbiol, and M. R. Ibarra, *Phys. Rev. B* **79**, 014431 (2009).
- [42] N. F. Mott and H. Jones, *The Theory of the Properties of Metals and Alloys* (Clarendon Press, Oxford, England, 1936), pp. 308–314.